Determining Disc Parameters in Planetary Images

SM51A-2300

P. Guio[1,2], N. Achilleos[1,2], L. Lamy[3] and R. Prangé[3]

[1] Department of Physics and Astronomy, University College London (UCL), UK; [2] Centre for Planetary Science, UCL/Birkbeck; [3] LESIA, France

Email contacts: p.guio@ucl.ac.uk, n.achilleos@ucl.ac.uk, laurent.lamy@obspm.fr, renee.prange@obspm.fr

Download poster from `http://www.ucl.ac.uk/~ucappgu`

Abstract

We present a semi-automatic image processing technique to estimate accurately, and objectively, the disc parameters of a planetary body on an astronomical image. The method relies on the detection of the limb and/or the terminator of the planetary body with the VOronoi Image SEgmentation (VOISE) algorithm [5]. The resulting map of the segmentation is then used to identify the visible boundary of the planetary disc. The segments comprising this boundary are then used to perform a "best" fit to an algebraic expression for the limb and/or terminator of the body. We test the method on a selection of Jupiter, Saturn and Uranus images taken by the Hubble Space Telescope (HST). The method is able to locate the centre of the planetary disc with an accuracy better than a pixel and thus represents a useful processing stage for auroral "imaging" based studies.

Introduction

During the last two decades, the Hubble Space Telescope (HST) has provided high sensitivity and high resolution ultraviolet (UV) images of the auroras on Jupiter and Saturn. Such images have become particularly useful for morphological studies of the aurora and its boundaries, which is crucial to identify the aurora's physical origin [4, 2, 1, 6]. Combining remote imaging with in situ plasma data (e.g. *Cassini* spacecraft) allows the study of magnetospheric processes and how they affect the planet's upper atmosphere. Such studies require accurate projection of the geographic and geomagnetic coordinate systems of the planet onto the image plane. For such applications the location of the planet centre needs to be accurate. Unfortunately, telescope pointing parameters are not generally accurate enough. The precision of the guide star catalogue is on the order of 1 arc sec while an accuracy of the order of 1 pixel is desired, i.e. 0.02–0.03 arc sec for the Space Telescope imaging spectrograph (STIS) and Advanced Camera for Surveys (ACS) instruments.

Planetary Disc Location Algorithm

The method is divided into three phases:

(i) Detection of the visible boundary of the planetary disc (limb and/or terminator) using our image segmentation algorithm VOronoi Image SEgmentation (VOISE) [5].

(ii) Selection of points (seeds of the Voronoi Diagram) from the VOISE map that surround the limb of the planetary disc.

(iii) Nonlinear "best" (geometrical) fit of the selected set of points to a parametrised model for the illuminated planetary disc.

(i) is performed once while (ii) and (iii) can be repeated in order to improve the accuracy.

Limb Equation

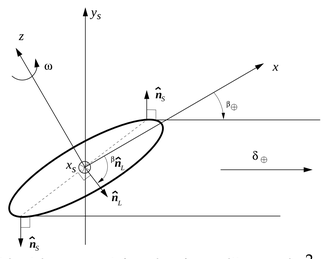

Fig. 1: The planet is an ellipsoid with equatorial and polar radii r_e and $r_p^2 = r_e^2(1-e^2)$. The z-axis is the planet's rotation axis. The observer is located in the (x,z)-plane, and the observing direction is defined by vector $\delta_\oplus$ with latitude $\beta_\oplus$.

The limb of the planet consists of the points on the planet surface where the local normal $\hat{n}_L$ is perpendicular to $\delta_\oplus$. The limb is an ellipse, lying in a single plane. The ellipse formed by the limb can then be projected onto the plane of the sky (x_s, y_s) which is perpendicular to the observing direction $\delta_\oplus$. The projection of the limb in the sky-plane is the ellipse written in the sky plane coordinate system

$$\frac{x_s^2}{r_e^2} + \frac{y_s^2}{r_e^2(1-e^2\cos^2\beta_\oplus)} = 1.$$

The limb always appears with a semi-major axis equal to the equatorial radius of the planet and a semi-minor axis between the polar and equatorial radii.

Terminator Equation

The terminator can be thought of as the limb for the direction corresponding to the direction of the Sun $\delta_\odot$ with local normal $\hat{n}_T$ and latitude $\beta_\odot$, but projected onto the sky plane along the Earthward observing direction $\delta_\oplus$. The Sun direction has a relative longitude to the observing direction $\Delta\lambda = \lambda_\odot - \lambda_\oplus$. The line with direction $\delta_\oplus \times \hat{n}_T$ intersects the limb projection and the terminator projection at two points called the cusps. The cusp points define the major axis of the ellipse formed by the terminator; this shape is an ellipse which is tilted by θ_T with respect to the x_s-axis

$$\theta_T = \tan^{-1}\left(\frac{\cos\beta_\odot \sin\Delta\lambda}{\cos\beta_\odot\cos\Delta\lambda\sin\beta_\oplus - \sin\beta_\odot\cos\beta_\oplus}\right).$$

The semi-major axis a_T and semi-minor axis b_T of the projection of the terminator onto the sky-plane are

$$a_T^2 = (u^2+v^2)t_1^2 \quad \text{and} \quad b_T^2 = (u^2+v^2)t_2^2,$$

where (u,v) is a vector co-linear to the direction $\delta_\oplus \times \hat{n}_T$

$$u = \cos\beta_\odot\cos\Delta\lambda\sin\beta_\oplus - \sin\beta_\odot\cos\beta_\oplus,$$
$$v = \cos\beta_\odot\sin\Delta\lambda,$$

and the values for t_1 and t_2 are analytically derivable from u and v.

Image Reduction Using Segmentation

VOronoi Image SEgmentation (VOISE) is a dynamic algorithm for partitioning the underlying pixel grid of an image into polygonal regions organised as a Voronoi diagram (VD) and according to a prescribed homogeneity criterion [5]. The transition region between the illuminated planet and the sky consists of a ring of very small Voronoi region (VR), indicating that the intensity of the image is changing sharply over small spatial scales.

Points Selection

The map generated at the division phase provides the largest number of seeds and smallest Voronoi polygons. The seed selection process requires a rough estimate of the planet centre and the equatorial and eventually the polar radii. The Voronoi region $\mathcal{R}(s_i)$ is in the neighbourhood of the limb/terminator if the following conditions are fulfilled

1. Its seed s_i is inside a prescribed "torus" (parametrised with inner and outer "scale" factors ε_m and ε_M).
2. Its length scale $\mathcal{L}_i$ is smaller than a prescribed length scale $\mathcal{L}_M$ (of the order of the minimum distance between seeds d_m prescribed during division phase of VOISE).

Filtering by "bands" of polar angle is also available in order to remove auroral emission outside the planetary limb.

Geometrical Best Fit To Primitive

Fitting algorithms for quadrics can be separated into two categories: "best fit" or "geometric fit", and "algebraic fit" [3]. In the "best fit", the geometric distance to the given points is minimised. Curves represented in parametric form, are well suited to minimise the sum of the squares of the distances. In the "algebraic fit", the curve is represented algebraically, i.e. by an equation of the form $F(x,y) = 0$. F is an algebraic distance and is minimised. *Disadvantage:* it is uncertain what is minimised in a geometrical sense. *Limitation:* can fit only one primitive at time.
We have developed a "best fit" for primitives in parametric form $(x,y) = \boldsymbol{f}(\phi;\boldsymbol{p})$ that minimises the weighted sum of the squares of the distances between seeds and the curve $\boldsymbol{f}$ by adjusting the set of parameters $\{\phi_i\}$ and $\boldsymbol{p}$

$$Q(\phi_1,\phi_2,\ldots,\phi_m,\boldsymbol{p}) = \sum_{i=1}^{m}\frac{\|\boldsymbol{s}_i - \boldsymbol{f}(\phi_i;\boldsymbol{p})\|^2}{\mathcal{L}_i^2}.$$

The length scale $\mathcal{L}_i$ of each Voronoi polygon $\mathcal{R}(s_i)$ is used as an estimate for the error on the position of the seed s_i. Note that *any subset of the parameters $\boldsymbol{p}$ can be fitted while the remaining parameters can be enforced*. For instance the planetary disc radii can be fitted and provide information about the limb altitude corresponding to the observed day glow emission.

Application to HST/ACS UV image

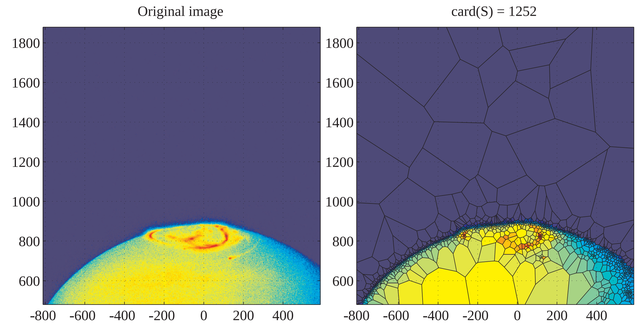

Fig. 2: In the upper panel, UV image collected by HST and in the lower panel the resulting Voronoi tessellation from the VOISE algorithm. The 1252 tiles of the tessellation are uniformly coloured using the median intensity of the pixels that are lying within each polygon. The axes are labelled in pixels unit and the point with coordinates $(0,0)$ is the centre of the planet provided with the image. The colour code for both images is shown in Fig. 4.

Seed Selection

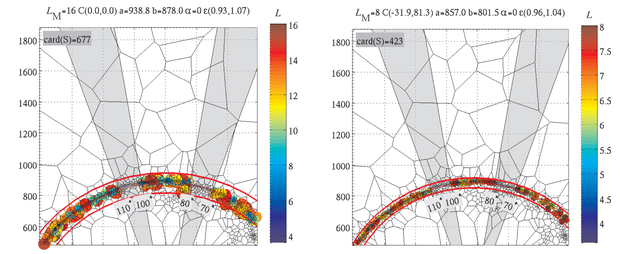

Fig. 3: Selection of the seeds from the VOISE tessellation for two iterations of the phases (ii) and (iii). During the first iteration (upper plot) 666 seeds are selected as neighbours of the limb while for the second iteration the numbers of seeds considered for the fit is reduced to 583 seeds. The size of each coloured marker is proportional to the surface area of the selected polygon. The limits of the annulus are shown in thick red lines while the nominal ellipse is shown as a thin red line and the red cross is the centre of the annulus.

Fit Result

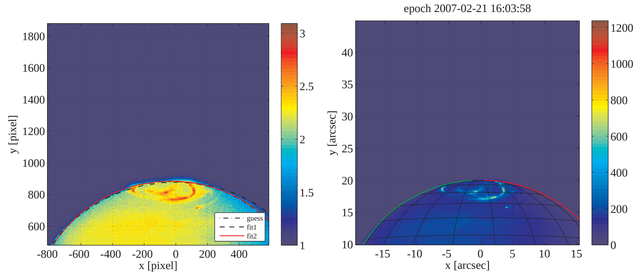

Fig. 4: Left: initial guess for the ellipse and the ellipses resulting from the two successive fits for the original image shown in Fig. 2. The points selected for each fit are as shown in Fig. 3. Right: Image scaled in arc sec and the projection in the sky-plane of a latitude-longitude grid of Jupiter computed using data from SPICE and the fitted parameters of Jupiter's disc.

	x_c	y_c	a	b	α	# iter	χ^2
guess	0.0	0.0	938.8	878.0	0		
fit 1	−31.9±1.4	81.3±4.6	857.0±4.3	801.5±4.1	0	4	10.91
fit 2	−30.4±1.4	83.5±4.4	856.5±4.1	801.1±3.8	0	3	8.23

Parameters of the fitted ellipse resulting from two iterations of phases (ii) and (iii). The ellipses are shown in Fig. 4. Note that the tilt angle α has not been fitted and has been fixed to $\alpha = 0$. # iter is the number of iterations performed in order to converge with the prescribed tolerance and the normalised χ^2 provides an indication of the goodness of the fit. The "guess", "fit 1" and "fit 2" ellipses are shown in Fig. 4.

References

[1] S. V. Badman, S. W. H. Cowley, L. Lamy, B. Cecconi, and P. Zarka. Relationship between solar wind corotating interaction regions and the phasing and intensity of Saturn kilometric radiation bursts. *Ann. Geophysicæ*, 26:3641–3651, November 2008.

[2] J. T. Clarke, J.-C. Gérard, D. Grodent, S. Wannawichian, J. Gustin, J. Connerney, F. Crary, M. Dougherty, W. Kurth, S. W. H. Cowley, E. J. Bunce, T. Hill, and J. Kim. Morphological differences between Saturn's ultraviolet aurorae and those of Earth and Jupiter. *Nature*, 433:717–719, February 2005.

[3] A. Fitzgibbon, M. Pilu, and R.B. Fisher. Direct least square fitting of ellipses. *IEEE Trans. Pattern Anal. Mach. Intell.*, 21(5):476–480, may 1999.

[4] D. Grodent, J. T. Clarke, J. Kim, J. H. Waite, and S. W. H. Cowley. Jupiter's main auroral oval observed with HST-STIS. *J. Geophys. Res.*, 108:1389–+, November 2003.

[5] Guio, P. and Achilleos, N. The VOISE Algorithm: a Versatile Tool for Automatic Segmentation of Astronomical Images. *Mon. Not. R. Astron. Soc.*, pages 1051–+, August 2009.

[6] L. Lamy, B. Cecconi, R. Prangé, P. Zarka, J. D. Nichols, and J. T. Clarke. An auroral oval at the footprint of Saturn's kilometric radio sources, colocated with the UV aurorae. *J. Geophys. Res.*, 114:10212–+, October 2009.